Korean J. Chem. Eng., 32(7), 1305-1313 (2015)
DOI: 10.1007/s11814-014-0340-8

pISSN: 0256-1115
eISSN: 1975-7220

Effect of the TiO_2 phase and loading on oxygen reduction reaction activity of PtCo/C catalysts in proton exchange membrane fuel cells

Napapat Chaisubanan*, Kejvalee Pruksathorn*,, Hugues Vergnes***, and Mali Hunsom*,**,†**

*Fuels Research Center, Department of Chemical Technology, Faculty of Science, Chulalongkorn University, 254 Phayathai Road, Bangkok 10330, Thailand
**Center of Excellence on Petrochemical and Materials Technology (PETRO-MAT), Chulalongkorn University, 254 Phayathai Road, Bangkok 10330, Thailand
***Laboratoire de Génie Chimique, UMR 5503 CNRS/ENSIACET/INPT, 4 Allee Emile Monso-CS 44362, 31030 Toulouse Cedex 4, France
(*Received 5 August 2014 • accepted 17 November 2014*)

Abstract−We investigated the effect of the TiO_2 phase, as either pure rutile (TiO_2(R)) or a 4 : 1 (w/w) anatase: rutile ratio (TiO_2(AR)), and the loading on the activity of PtCo/C catalyst in the oxygen reduction reaction (ORR) in a proton exchange membrane (PEM) fuel cell. The incorporation of the different phases and loading of TiO_2 on the PtCo/C catalyst did not affect the alloy properties or the crystalline size of the PtCo/C catalyst, but affected importantly the electrochemical surface area (ESA), conductivity of catalyst layer and the water management ability. The presence of TiO_2(AR) at appropriate quantity can decrease the mass transport limitation as well as the ohmic resistance of catalyst layer. As a result, the optimum loading of TiO_2(AR) used to incorporated in the layer of PtCo/C catalyst was 0.06 mg/cm^2. At this content, the TiO_2(AR)-PtCo/C catalyst provided the highest current density of 438 mA/cm^2 at 0.6 V at atmospheric pressure in PEM fuel cell and provided the kinetic current in acid solution of 20.53 mA/cm^2. In addition, the presence of TiO_2(AR) did not alter the ORR electron pathway of PtCo/C catalyst. The electron pathway of ORR of TiO_2(AR)-PtCo/C was still the four-electron pathway.

Keywords: PEM Fuel Cell, ORR Activity, TiO_2, Mass Transport Limitation

INTRODUCTION

Proton exchange membrane (PEM) fuel cells are currently the most competitive candidates to replace traditional forms of power conversion due having zero emissions, high efficiency and a relatively simple design and operation [1,2]. They are able to meet transportation and stationary power requirements owing to their low operating temperature, quick start, light weight and high power density [3]. However, the commercialization and utilization of PEM fuel cells is still not currently widespread because of the two major technical gaps of their high cost and low reliability/durability [4].

Practically, highly dispersed platinum (Pt) crystallites on a conductive carbon support, such as Vulcan XC-72 (C), are utilized as catalyst in fuel cells because Pt has a high exchange current density for both the oxidation and reduction reactions in the fuel cell, a high resistance to chemical attack, excellent high-temperature characteristics and stable electrical properties [5]. However, Pt is expensive and is in demand for other applications; the world's supply of Pt is limited, resulting in a high production cost for fuel cells. Thus, many strategies have been considered to reduce the amount of Pt catalyst consumption in a fuel cell, such as the development of new Pt-based catalysts that have a higher mass activity, improved catalyst and microporous layer structures, diffusion media, flow field design and durability of the catalyst and support [6]. Over the past decade, several classes of less precious and non-precious metal catalysts have been investigated in order to try to attain a more cost-effective and active cathode for PEM fuel cells. These have included Ru, Pd, Au and Ag [7-9], chalcogenides [10-14], nitrides [15,16], functionalized carbons [17-20] and the macrocyclic non-precious electrocatalysts [11,21-28]. However, these approaches are still in the research stages and are currently far from commercially viable.

Another strategy is the development of bimetallic alloy electrocatalysts with Pt and another metal (Pt-M). Several works have pointed out that the ORR activity of a Pt catalyst can be enhanced by the presence of a composite metal (as a Pt-M alloy catalyst) because the composite metal can modify the geometrical structure of Pt by decreasing the Pt-Pt bond distance [29], dissolution of the more oxidizable alloying component [30], and changing the surface structure [31] or the electronic structure by increasing the Pt *d*-electron vacancy [32]. This high ORR catalytic efficiency is caused by the facilitation of O_2 interactions with the adsorption sites (or active sites) on the surface of the catalyst, indicating that both electronic and geometric factors affect the level of -OH chemisorption and kinetics of the ORR [33].

Recently, most research has focused on the mixing of metal oxides with commonly used carbon supports [34] or even substituting the carbon by the doped metal oxides [35-38] to improve the catalyst's stability. However, only a few have attempted to improve the

†To whom correspondence should be addressed.
E-mail: mali.h@chula.ac.th

ORR activity by the addition of a metal oxide, such as MoO_x, TiO_x and CeO_x, on the Pt/C catalyst [33,39]. In addition, most studies have focused on the direct methanol fuel cell (DMFC). No work in the literature has reported on the incorporation of a metal oxide on a Pt-M alloy catalyst for PEM fuel cells to improve the ORR activity.

To explore the effect of the addition of a metal oxide on the ORR activity of a Pt-based catalyst in PEM fuel cells, we selected titania (TiO_2) as the candidate metal oxide and coated onto the PtCo/C catalyst. It was expected that the presence of an appropriate quantity of TiO_2 on the PtCo/C catalyst layer would enhance the ORR activity owing to its water management ability due to its hydrophilic properties [40] and probably the formation of the interface between the Pt and oxide materials and the spillover behavior [33].

EXPERIMENTAL

1. Preparation of the PtCo/C Catalyst

During the preparation of each electrocatalyst, two elementary steps of seeding and impregnation were performed [41]. Initially, 0.1 g of carbon black (Vulcan XC-72), pretreated in a 7 : 3 (v/v) ratio of conc. HNO_3 : H_2SO_4 as previously reported [42], was dispersed in 3 mL of de-ionized water to obtain a 1% (w/v) carbon slurry, sonicated at 70 °C for 1 h and then the solution was adjusted to pH 2 with 13.3 M HCl.

The seeding step was conducted by mixing the PtCo precursor (2.844 mL of 20 g/L $H_2PtCl_6{\cdot}6H_2O$ (Fluka) and 4.324 mL of 20 g/L $CoCl_2$ ($CoCl_2{\cdot}6H_2O$, Kanto Chemical)) with the above 10% (v/v) carbon black slurry and sonicated at 70 °C for 30 min. The metal ions in the aqueous solution were then reduced to PtCo metal by the addition of 20 mL of 0.12 M $NaBH_4$ (98%, Alcan) and sonicated for 30 min at 70 °C. The insoluble fraction was harvested by filtration and rinsed several times with de-ionized water to eliminate the excess reducing agent.

The impregnation step was performed by dispersing the obtained carbon powder covered by the seeded PtCo metal in de-ionized water, sonicating for 1 h and then adding to the remaining H_2PtCl_6 and $CoCl_2{\cdot}6H_2O$ (90% (v/v)) solution to obtain the required electrocatalyst loading on the carbon support (30% (w/w)). The mixture was reduced by the addition of 20 mL of 0.12 M $NaBH_4$ and sonicated for 30 min to obtain the catalyst powder, which settled out of the solution/suspension. The electrocatalyst suspension was filtered, and the filtrate was washed thoroughly with hot de-ionized water and dried for 2 h at 110 °C.

2. Preparation of the Sublayer, Catalyst Ink and Catalyst-coated Membrane

The sublayer was prepared by mixing 0.5 mL of distilled H_2O with 1.334 μL of 60% (w/w) polytetrafluoroethylene (Aldrich) and sonicating at room temperature (~30 °C) for 30 min. The mixed solution was added to 1.0 mL of *i*-propanol (99.99% C_3H_7OH, Fisher) and sonicated again at room temperature for 30 min. Next, 18.0 mg of treated carbon was added and sonicated at room temperature for 30 min to obtain the carbon ink, which was then coated onto a 2.25×2.25 cm gas diffusion layer (GDL) (Carbon cloth, ETEK) by brushing and then dried at 80 °C for 2 min to eliminate the excess solvent. The carbon ink coating was repeated as required until the sublayer loading was ~2.0 mg/ cm^2, and then the sublayer ink-coated GDL was dried at 300 °C for 1 h at atmospheric pressure (~101.3 kPa).

The catalyst ink was prepared by mixing 0.1 g PtCo/C catalyst powder with 0.4 mL of distilled H_2O and then sonicated at room temperature (~30 °C) for 30 min. The obtained mixture was added into 0.916 mL Nafion solution (5% (w/v) Nafion117, Fluka), sonicated at the same temperature for 1 h, and then 3.2 mL of *i*-propanol (99.99% C_3H_7OH, Fisher) was added and the solution was sonicated for 1 h.

The membrane electrode assembly (MEA), with a 5 cm^2 active surface area, was prepared as the catalyst-coated membrane by direct spraying with a spray gun (Crescendo, Model 175-7^{TM}) onto the pretreated membrane (Nafion 115) at 80 °C. For the cathode, the PtCo/C catalyst ink was sprayed slowly and then left at room temperature for 3-5 min to obtain a dry layer. The coating process was repeated several times to reach a catalyst loading of 0.15 mg/cm^2 and then dried at 80 °C for 10 min. A similar spraying procedure was done with the TiO_2 slurry, obtained by mixing 2.5 mg of commercial TiO_2, as either the 100% rutile phase (TiO_2(R)) (particle size of 18.7 nm) or a 4 : 1 (w/w) anatase: rutile phase ratio (TiO_2(AR)) (particle size of 22.9 nm), with 6 mL *i*-propanol (99.99% C_3H_7OH, Fisher), until the required loading density was obtained (0.06-0.45 mg/cm^2). This procedure was repeated for the anode side but using only the commercial Pt/C (20% (w/w), ETEK) at a loading density of 0.15 mg/cm^2. Finally, the membrane was assembled between two sheets of sublayer ink-coated GDL and pressed together by a compression mold (LP20, Labtech) under 65 kg/cm^2 for 2.5 min at 137 °C.

3. Electrode Characterization

The morphology of all as-prepared catalysts, including the evaluation of the crystalline size and *d*-spacing together with the metal content, was analyzed by X-ray diffractometry (XRD, D8 Discover-Bruker AXS) and scanning electron microscopy (SEM) with energy dispersive X-ray spectroscopy (EDX) on a JSM 6400 machine, respectively. The in-plane conductivity of the catalyst layer was evaluated with a fully-hydrated specimen using a 4-probe apparatus (RM3-AR).

The ESA was estimated from the H_2 stripping method in N_2-saturated 0.5 M H_2SO_4. Initially, the catalyst ink prepared as described in section 2.2 was coated on the GDL substrate, cut as a square sheet with a dimension of 1×1 cm, and mounted with a home-made measuring template. The as-prepared catalyst-coated substrate, a Pt gauze and saturated calomel electrode (SCE) were used as working-, counter- and reference electrodes, respectively. The potential was varied between −0.24 to +1.00 V at a scan rate of 20 mV/s using a potentiostat/galvanostat (DEA332, Radiometer). The ESA of catalyst can be estimated from the hydrogen desorption peak according to Eq. (1) [43]:

$$\mathrm{ESA} = \frac{Q_H}{[\mathrm{M}] \times 0.21} \tag{1}$$

where Q_H is the charge for hydrogen desorption, 0.21 is the charge required to oxidize a monolayer of H_2 on bright Pt and [M] is the metal loading of Pt on the electrode.

4. ORR Activity Test

The ORR activity test of as-prepared electrocatalysts was carried

out in two procedures, including the activity test in single PEM fuel cell under the H_2/O_2 environment and the test in O_2-saturated 0.5 M H_2SO_4 using a rotating disk electrode (RDE). For the first test, the obtained MEA of each catalyst with a constant active surface area of 5 cm^2 was mounted on commercial single-cell hardware (Electrochem, Inc.) and tested in a single-cell test station. Prior to testing the cell performance, the run-in stage was performed under atmospheric pressure (~101.3 kPa) with a cell temperature of ~60 °C by feeding H_2 and O_2 at 100 sccm each (100% humidity). The current was drawn at a high density (>700 mA/cm^2) for 6-12 h. Subsequently, the performance of the single cell was evaluated in the form of current-density-potential curves, monitored by a potentiostat/galvanostat at 60 °C and ambient pressure. For the second test, the catalyst ink prepared as described in section 2.2 was coated on the carbon cloth (E-TEK). The catalyst-coated carbon cloth was cut as a 1 cm diameter circular sheet and assembled with the rotating disk substrate. Subsequently, it was connected to the potentiostat/galvanostat as the working electrode. A Pt gauze and SCE reference electrode were used as the counter and reference electrodes, respectively. The potential was varied from −0.20 to 0.70 V, at different rotation rates ranging from 500-2,000 rpm and a constant sweep rate of 10 mV/s.

RESULTS AND DISCUSSION

1. Morphology of the As-prepared Electrodes

Representative XRD patterns of the commercial Pt/C (ETEK) and all PtCo/C catalysts, both in the absence and in the presence of TiO_2, are demonstrated in Fig. 1. The commercial Pt/C (ETEK) electrocatalyst exhibited four main peaks. The first peak at a 2θ value of about 24.67° was due to the presence of the carbon support in the hexagonal structure [44]. The other three peaks are the characteristic peaks for the diffraction pattern of face-centered cubic (FCC) Pt [45], corresponding to the [111], [200] and [220] planes at a 2θ of 39.67°, 45.80° and 67.78°, respectively. The diffraction peak of the as-prepared PtCo/C catalyst still demonstrated the characteristic FCC crystalline Pt. However, compared with the diffraction of the bulk Pt, its diffraction peaks were shifted slightly to higher 2θ values (40.6°, 47.04° and 68.40°). In addition, the *d*-spacing value

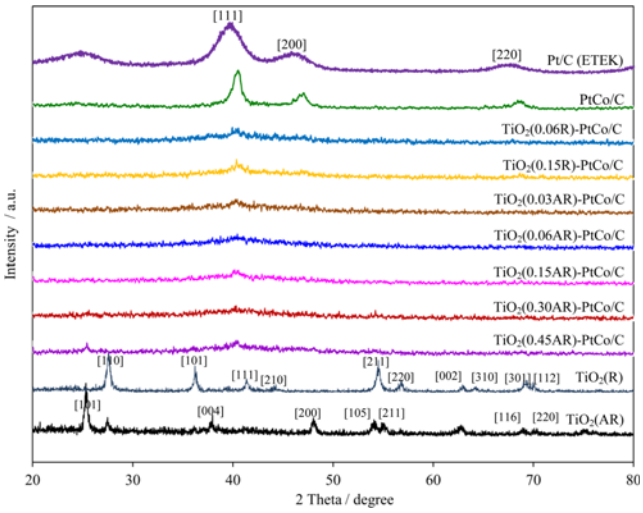

Fig. 1. Representative XRD patterns of the commercial Pt/C (ETEK) and the as-prepared PtCo/C catalysts in the absence or presence of TiO_2(R) or TiO_2(AR) at different loadings.

for the as-prepared PtCo/C catalysts (Table 1) was smaller than that of the commercial Pt/C catalyst. Both parameters indicated the formation of a PtCo alloy due to the particle substitution of Pt by Co in the FCC structure [46]. Although no characteristic peaks of metallic Co or its respective oxides were detected in the XRD plots of the PtCo/C catalysts, their presence could not be formally excluded because they may be present in a very small amount and/or in an amorphous form. By using the EDX analysis, it exhibited the uniform distribution of both metal particles along the GDL surface (Fig. 2(a)). The presence of Pt particles was slightly denser than that of Co, referring the presence of a higher quantity of Pt particles than Co. Quantitatively, the Pt : Co ratio in the PtCo/C catalyst was around 58.5 : 41.5.

When TiO_2(R) or TiO_2(AR) was incorporated onto the surface of PtCo/C catalyst, their XRD patterns also exhibited the characteristic Pt peaks of a FCC structure (Fig. 1). However, the XRD features for TiO_2 were only observed at a high TiO_2 loading (0.45 mg/cm^2), which might be attributed to the presence of TiO_2 in a very

Table 1. Morphology of the Pt/C- and PtCo/C-catalyst layer at different TiO_2 loadings

Type of catalyst[a]	*d*-Spacing (nm)	Crystalline size (nm)	ESA (m^2/g)	$j_{0.9\ V}$ (mA/cm^2)	$j_{0.6\ V}$ (mA/cm^2)	σ_{wet}[b] (mS/cm)
Pt/C (ETEK)	0.2264	2.78	44.8	13.2	395.8	
PtCo/C	0.2231	7.67	47.3	14.4	321.2	30.19
TiO_2(0.06R)-PtCo/C	0.2235	7.68	43.7	13.2	309.2	18.93
TiO_2(0.15R)-PtCo/C	0.2227	7.51	36.9	12.6	301.8	11.79
TiO_2(0.03AR)-PtCo/C	0.2238	7.69	27.7	15.2	366.2	17.00
TiO_2(0.06AR)-PtCo/C	0.2237	7.44	72.2	18.4	437.6	25.00
TiO_2(0.15AR)-PtCo/C	0.2235	7.41	71.8	20.2	435.8	14.83
TiO_2(0.30AR)-PtCo/C	0.2234	7.84	32.3	21.6	412.4	6.24
TiO_2(0.45AR)-PtCo/C	0.2244	7.74	31.0	22.2	371.4	5.59

[a]Numbers in parenthesis after TiO_2 refer to the TiO_2 loading in mg/cm^2, while the capital letters refer to its phase as (R) rutile or (AR) a 4 : 1 (w/w) anatase : rutile ratio

[b]In-plane measurement of the fully-hydrated catalyst layer

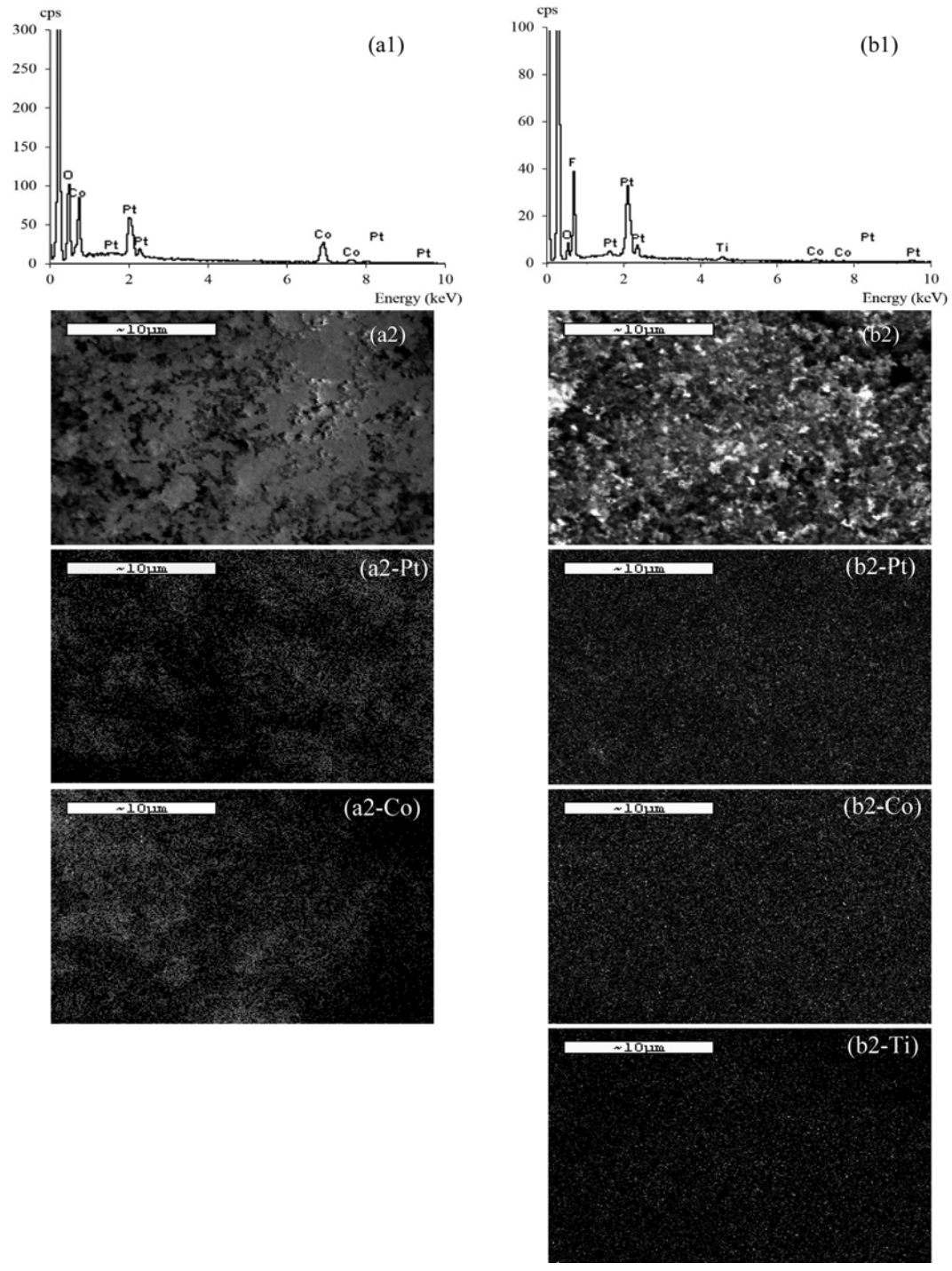

Fig. 2. EDX spectra of elements ((a1) and (b1)), SEM micrographs of crystalline particles ((a2) and (b2)), and X–ray images used to map the location of the elements dispersion (Pt, Co and Ti) of (a) Pt-Co/C and (b) TiO_2(0.06AR)-PtCo/C catalysts.

small amount and/or in an amorphous form. The *d*-spacing values of all TiO_2-PtCo/C catalysts were still lower than that of the commercial Pt/C and were broadly similar to that of the PtCo/C catalyst, indicating that the incorporation of TiO_2 on the surface of PtCo/C had no effect on the alloy property of the PtCo/C catalysts. By using the Debye-Scherrer equation, the crystalline size for the PtCo particles in the PtCo/C catalyst was determined to be 7.67 nm, which was 2.75-fold larger than that of the commercial Pt/C catalyst (Table 1). The incorporation of either TiO_2(R) or TiO_2(AR) had no significant influence on the crystalline size of PtCo/C catalysts. They deviated in the range of 7.41-7.84 nm (Table 1).

The existence of the Ti particle in the layer of TiO_2-PtCo/C catalyst was also confirmed by the SEM-EDX analysis (Fig. 2(b)). It exhibited a uniform distribution of Ti particles on GDL surface. As demonstrated in Fig. 3, the EDX-line scan of the cross-sectional TiO_2-PtCo/C catalyst revealed the presence of dense Ti particles at

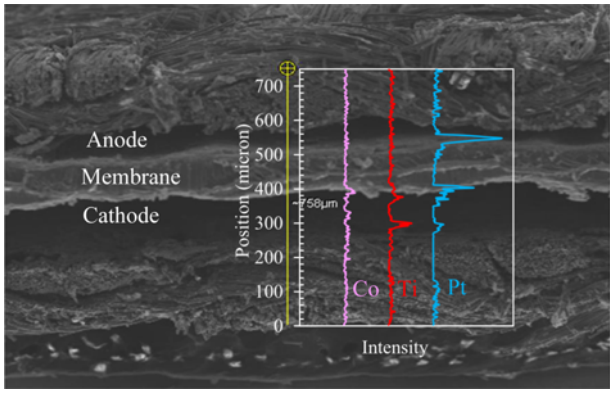

Fig. 3. Representative SEM micrograph (1,400 x magnification) of the cross-section of TiO_2(0.06AR)-PtCo/C catalyst, and (inset) the EDX-derived line scan of Pt, Co and Ti particles.

the cathode region (MEA depth of 300 μm) intermixed with lean Pt and Co particles. The cumulative presence of Pt particles was observed at an MEA depth of 380-400 μm beneath the Ti layer and, especially, again at 200-230 μm in the anode region. The Co particles were observed only on the cathode, interwoven with particles beneath the Ti layer. This shows that the PtCo/C catalysts were partially covered by the corresponding TiO_2. Also from Fig. 3, a very rough electrode surface was observed in the presence of TiO_2. Thus, the amount of ESA might change with the TiO_2 loading. To prove this hypothesis, a measurement of ESA of all as-prepared PtCo/C catalysts both in the absence and presence of TiO_2 at any phases and loadings was carried out in N_2-saturated 0.5 M H_2SO_4. As shown in Table 1, the presence of TiO_2(AR) provided both positive and negative impacts on the ESA of PtCo/C catalyst. Increasing the TiO_2(AR) from 0 to 0.06 mg/cm^2 resulted in increasing of ESA. However, further raising the TiO_2(AR) loading up to 0.45 mg/cm^2 led to the decreasing of ESA. The increasing ESA at low TiO_2(AR) content might be attributed to the increase of electrode roughness. Overloading of TiO_2(AR), particularly at 0.3 and 0.45 mg/cm^2 induced the blockage of percolating electron-conducting network in the electrode, resulting in a decreased electronic conductivity as well as ESA (Table 1).

2. ORR Activity Test in Single PEM Fuel Cell

The activities of the as-prepared PtCo/C-, TiO_2(R)-PtCo/C- and TiO_2(AR)-PtCo/C catalysts in the ORR were tested in a single PEM fuel cell at 60 °C and atmospheric pressure (~101.3 kPa) under a H_2/O_2 condition. As demonstrated in Fig. 4, the major reason for the power performance difference was the difference in ohmic resistance and mass transport resistance. The inclusion of either TiO_2(R) or TiO_2(AR) in the PtCo/C catalyst layer did not significantly affect the open circuit potential of the single cell, but significantly affected the cell performance, particularly at medium-to-high current densities.

Under the activation-controlled region, the presence of TiO_2(R) slightly changed the ORR activity, determined in terms of the current density at a potential of 0.9 V ($j_{0.9\ V}$) [47], of the PtCo/C catalysts. However, the presence of TiO_2(AR) enhanced the activity of the PtCo/C catalysts. Under a medium-to-high current density, the inclusion of TiO_2(AR) into the PtCo/C catalyst layer provided a higher current density compared to that in the presence of TiO_2(R) at the same loading. For example, at a loading of 0.06 mg/cm^2, replacing the TiO_2(R) by TiO_2(AR) increased the current density at 0.6 V ($j_{0.6\ V}$) of some 1.42-fold from 309 to 438 mA/cm^2 (186 to 263 mW/cm^2), while increasing the TiO_2(AR) content from 0.03 to 0.06 mg/cm^2 increased the current density at 0.6 V of around 1.19-fold (Table 1 and Fig. 5). However, further increasing the TiO_2(AR) loading from 0.06 to 0.45 mg/cm^2 decreased the current density by approximately 1.18-fold. To explain the effects of the TiO_2 phase and loading on the performance of the PEM fuel cell during the medium-to-high current density, it is necessary to take into account the composition and property of TiO_2. The electrical conductivity of a TiO_2(R)-based mixed oxide was reported to be higher than a non-crystalline or TiO_2(A)-based mixed oxide [35], while TiO_2(A) exhibits hydrophilic behavior [48]. Although the incorporation of TiO_2(AR) could reduce the electrical conductivity of the catalyst layer, because of its low electrical conductivity compared to the carbon support and metal catalysts, an appropriate quantity of TiO_2(AR) can improve the hydrophilic properties of the catalyst layer and also prevent the drying out of the membrane, which results in an increased proton conductivity. This was supported by the increased performance of the single cell when the TiO_2(AR) loading was increased from 0.03

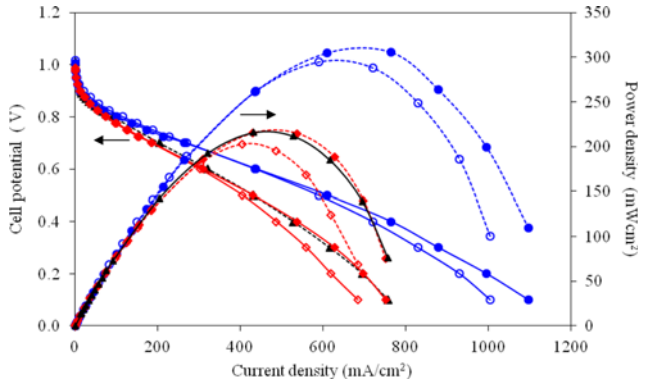

Fig. 4. Current density-potential curves of a single H_2/O_2 PEM fuel cell with the as-prepared PtCo/C catalyst in the (▲) absence of TiO_2, and in the presence of (●, ○) TiO_2(R) or (◇, ◆) TiO_2(AR) at a loading of (●, ◆) 0.06 and (○, ◇) 0.15 mg/cm^2.

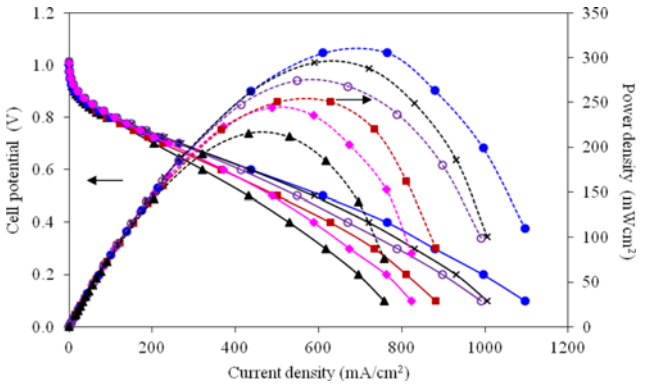

Fig. 5. Current density-potential curves of a single H_2/O_2 PEM fuel cell of the as-prepared TiO_2(AR)-PtCo/C catalyst at TiO_2 loadings of (▲) 0.0, (■) 0.03, (●) 0.06, (×) 0.15, (○) 0.30 and (◆) 0.45 mg/cm^2.

Table 2. Electrode kinetics and mass transport parameters, obtained from fitting the polarization data of Eq. (2), for the different types of supported PtCo/C catalysts

Type of catalyst[a]	Activation loss		Ohmic loss	Mass transport loss		R^2
	−b (mV/dec)	j_0 (A/cm^2)	R (Ω-cm^2)	m (mV)	n (cm^2/mA)	
PtCo/C	67.0	7.19×10^{-7}	0.7000	0.0015	0.0062	0.9992
TiO_2(0.03AR)-PtCo/C	69.5	8.78×10^{-7}	0.5572	0.0008	0.0060	0.9994
TiO_2(0.06AR)-PtCo/C	69.9	9.61×10^{-7}	0.5050	0.0005	0.0052	0.9995
TiO_2(0.15AR)-PtCo/C	66.4	9.93×10^{-7}	0.5100	0.0015	0.0047	0.9997
TiO_2(0.30AR)-PtCo/C	63.4	9.92×10^{-7}	0.5860	0.0029	0.0043	0.9999
TiO_2(0.45AR)-PtCo/C	66.1	9.93×10^{-7}	0.5890	0.0052	0.0045	0.9992

[a]Numbers in parentheses after TiO_2 refer to the TiO_2 loading in mg/cm^2, while the letters refer to its phase as (R) rutile or (AR) a 4 : 1 (w/w) anatase : rutile ratio

to 0.06 mg/cm^2. However, too high loading of TiO_2(AR) (>0.06 mg/cm^2) induced a diminished fuel cell performance because it functioned as an insulating phase in the catalyst layer, resulting in the reduction of the electrical conductivity of the catalyst layer (Table 1). In addition, a high TiO_2 content can induce a high mass transport limitation because it could combine or adsorb a large quantity of water molecules and so hinder the accessibility of the fuel gas/oxidant to the reaction site. Another possible reason might be that, under an oxygen atmosphere, TiO_2 can adsorb oxygen molecules, which then captures electrons from the conduction band and the donor states of TiO_2 to form O_2^- and so causes a decreased dark conductivity [49,50]. Although the presence of TiO_2(AR) at 0.03 to 0.45 mg/cm^2 reduced the electrical conductivity of the TiO_2(AR)-PtCo/C catalyst 1.78- to 5.40-fold, the cell performance at 0.6 V was still 1.14- to 1.36-fold higher than that of the PtCo/C catalyst (Table 1). This indicates that the hydrophilic property of TiO_2(AR) plays an important role in the performance of the fuel cell, particularly at a medium-to-high current density.

To further understand the effect of the TiO_2(AR) loading on the kinetic and mass transport parameters of the electrode, we evaluated the relationship between the cell potential and current density for the entire current density range using a non-linear least squares approach, as expressed by Eq. (2) [51]:

$$E=E_0-b\log j-jR-m\exp(nj) \quad (2)$$

where $E_0=E_r+b\log j_0$; E_r is the reversible potential for the cell; b is the Tafel slope for the ORR; R is all the resistances due to the ohmic resistance contributed from the proton transfer through membrane and the electron transfer through the fuel cell components, and the mass-transport resistance in the intermediate current density region; j is the current density; j_0 is the exchange current density, and m and n are the parameters related to the mass transport limitation and mass-transport overpotential, respectively. The m value affects both the slope of the linear region of the current density-potential plot and the region where the current density departs from linearity, whereas the n value has a major effect on the dependence of the current density-potential curve after the linear region [51]. High values of m and n indicate a high mass transport limitation and mass-transport overpotential in the system, respectively.

The fitted results, together with the coefficient of determination (R^2), are summarized in Table 2. The R^2 values for all catalysts were greater than 0.9992, indicating that the fitted model was adequate to predict the experimental data. Within the fitting error, the intrinsic Tafel slopes (b) for the ORR varied between −63.4 to −69.9 mV/dec under identical testing conditions. These changes can be attributed to the variation in the interphase conditions in the presence of different loadings of TiO_2(AR). Theoretically, a Tafel slope of −60 mV/dec indicates an ORR mechanism involving an initial fast charge-transfer step followed by the rate-determining chemical step [52]. A higher Tafel slope value is found at low O_2 concentrations due to mixed activation/mass-transport control. The exchange current density (j_0) was found to increase as the TiO_2(AR) loading increased up to 0.15 mg/cm^2 and remained essentially constant thereafter with further increases in the TiO_2(AR) loading. This is consistent with the ORR activity estimated at 0.9 V ($j_{0.9\ V}$) as reported in Table 1.

The variation of the resistance (R) and mass transport limitation parameters (m and n) as a function of the TiO_2(AR) loading are plotted in Fig. 6. The incorporation of TiO_2(AR) at a loading of between 0.03 to 0.06 mg/cm^2 resulted in a 1.10-, 1.60- and 1.15-fold decrease in the R, m and n parameters, respectively. Further increasing the TiO_2(AR) loading on the PtCo/C catalyst from 0.06 to 0.45 mg/cm^2 slightly decreased n by 1.16-fold, but increased R and m by 1.17 and 10.4-fold, respectively. Thus, a high TiO_2 content induced a high mass transport limitation, which, as mentioned

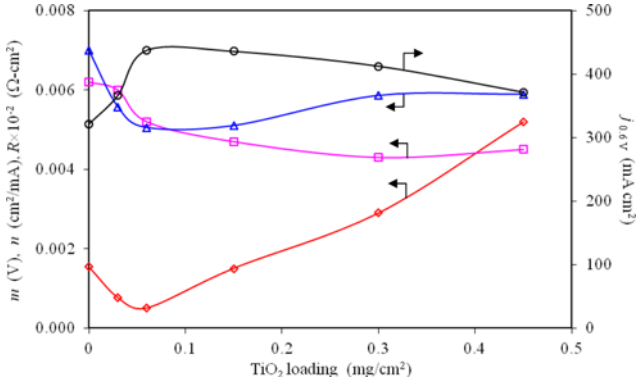

Fig. 6. Variation in the (◇) m, (□) n and (△) R parameters, as estimated from Eq. (2), and the (○) current density at 0.6 V ($j_{0.6\ V}$) for the TiO_2(AR)-PtCo/C catalyst at different TiO_2 loadings.

previously, may be because a high quantity of TiO_2(AR) particles can combine or adsorb a large quantity of water molecules and so hinder the accessibility of the fuel/oxidant to the reaction site. In addition, the TiO_2(R) particles can absorb water molecules from the membrane layer and so decrease the proton conduction of the membrane [53]. A decreased proton conductivity with increasing TiO_2(AR) loadings has been reported previously for the addition of a nano-TiO_2 film onto the membrane surface [54]. The high TiO_2(AR) content reduced the electronic conductivity of the catalyst (Table 1) because it functioned as an insulating phase, as mentioned previously. In addition, a high TiO_2 content can adsorb a high quantity of oxygen from the reactant feed, resulting in a loss of electrons from the conduction band and donor state and so a decreased conductivity [49, 50]. Accordingly, the addition of an appropriate quantity of TiO_2(AR) on the PtCo/C catalyst can help to decrease the mass transport limitation as well as the ohmic resistance of the catalyst layer.

3. ORR Activity Test in Acid Solution

Besides the activity in the PEM fuel cell, the ORR activity of all TiO_2(AR)-PtCo/C catalysts was tested in O_2-saturated 0.5 M H_2SO_4 using RDE at rotation rates between 500-2,000 rpm during a varying potential of −0.20 to 0.70 V and a constant sweep rate of 10 mV/s. A similar pattern of the voltammogram for the ORR was obtained for all TiO_2(AR)-PtCo/C catalysts as demonstrated in Fig. 7. The curve can be divided into three distinct regions. The first region is a kinetics-controlled region, where the current density is not affected by the rate of mass transfer, and it is independent of the rotation rate (ω). The second region is an intermediate region of mixed control where the current is partially controlled by mass transport and partially by the kinetics of electron transfer. The current increases with ω, but not as a linear function of $\omega^{1/2}$. The last region is a diffusion-controlled region, which shows a well-defined limiting current plateau that increased linearly with $\omega^{1/2}$.

The relation between the current density and the rotation rate can be expressed by the Koutecky-Levich equation (Eq. (3)). This equation is valid for a first-order process with respect to the diffusion species [55]:

$$\frac{1}{j} = \frac{1}{j_k} + \frac{1}{B\omega^{1/2}} \quad (3)$$

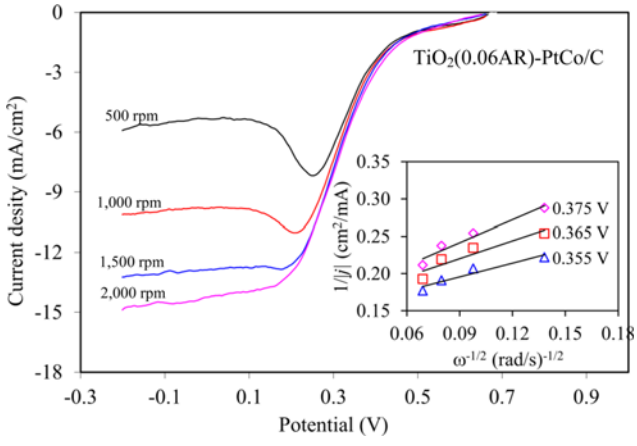

Fig. 7. Example of voltammogram for the ORR of TiO_2-PtCo/C catalyst and (insert) the Koutecky-Levich plots.

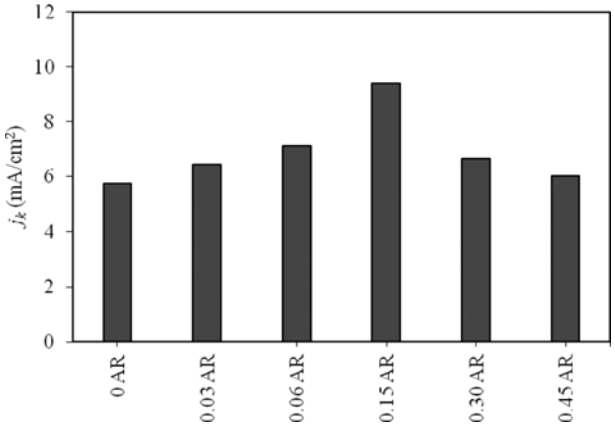

Fig. 8. Kinetically controlled ORR at 0.375 V versus SCE electrode for PtCo/C catalyst in the presence of different TiO_2 loadings.

and where B is estimated by Eq. (4),

$$B = 0.62 n_e F D^{2/3} \nu^{-1/6} C \quad (4)$$

Here, j_k is the kinetic current density, ω is the rotation rate, n_e is the number of involved electrons, F is Faraday's constant (96,485 C/mol), D is the diffusion coefficient of oxygen in solution (1.9×10^{-5} cm^2/s), ν is the kinematics viscosity (0.01 cm^2/s) and C is the oxygen concentration in the bulk solution (1.1×10^{-6} mol/cm^3).

The plot of j^{-1} vs. $\omega^{-1/2}$ provided straight lines with the intercepts corresponding to the kinetic current density (j_k), and a slope of 1/B could be determined (Fig. 7, insert). Fig. 8 shows the plot of kinetic current density of all TiO_2(AR)-PtCo/C catalysts. The increase in the ORR activity or j_k was found to depend on the loading of TiO_2(AR). Nevertheless, too high quantity of TiO_2(AR) cannot enhance the ORR activity. Just a certain quantity of TiO_2(AR) is required to promote the ORR activity. The highest ORR activity for PtCo/C catalyst was observed in the presence of TiO_2(AR) at the loading of 0.15 mg/cm^2, consistent with ORR activity determined in PEM fuel cell under H_2/O_2 environment at 0.9 V ($j_{0.9\ V}$) (Table 1).

Besides, from the Koutecky-Levich plots, the number of electrons transferred for the ORR on the as-prepared catalysts can be estimated from a slope of 1/B. From the calculation, the number of transferred electrons in the process via TiO_2(AR)-PtCo/C catalyst is between 3.84 and 3.97 with an average value of 3.91, suggesting that the ORR reaction occurred via the four-electron pathway.

From the ORR activity test, although the TiO_2(0.06AR)-PtCo/C catalyst exhibited a lower kinetic current density (7.10 mA/cm^2) than that of TiO_2(0.15AR)-PtCo/C catalyst (9.39 mA/cm^2) in acid solution, it provided a slightly higher current density at 0.6 V tested in PEM fuel cell (Table 1). For actual application of such catalyst, the performance in the PEM fuel cell should be considered first. Thus, it can be said that the optimum TiO_2(AR) in PtCo/C catalyst for ORR in PEM fuel cell was 0.06 mg/cm^2.

CONCLUSIONS

The effect of the TiO_2 phase and loading on the activity of a PtCo/C catalyst for the ORR in a single cell PEM fuel cell was studied. The incorporation of either TiO_2(R) or TiO_2(AR) on PtCo/C cata-

lysts at different loadings onto the surface of PtCo/C catalyst did not affect the alloy properties of the PtCo/C catalyst layer or the crystalline size, but altered the ESA and the ORR activity. The addition of TiO_2(AR) at a certain value (0.06-0.15 mg/cm^2) can enhance the ORR activity in PEM fuel cell as well as in acid solution due to the decrease of mass transport limitation as well as the ohmic resistance of catalyst layer. In summary, for the actual application in PEM fuel cell, the optimum loading of TiO_2(AR) in PtCo/C catalyst was selected at 0.06 mg/cm^2. At this content, the TiO_2(AR)-PtCo/C catalyst provided the highest current density of 438 mA/cm^2 at 0.6 V, which was greater than that of Pt/C (ETEK) and PtCo/C catalysts of 1.11- and 1.36-fold, respectively. The ORR via TiO_2(AR)-PtCo/C followed the four-electron pathway.

ACKNOWLEDGEMENTS

The authors thank the Royal Golden Jubilee Ph.D. Program of the Thailand Research Fund (Grant No. PHD/0338/2552) and the Embassy of France in Thailand for financial support, and the Publication Counseling Unit (PCU) of the Faculty of Science, Chulalongkorn University, and Dr. Robert D.J. Butcher for comments, suggestions and checking the grammar.

REFERENCES

1. J. H. Lin, W. H. Chen, Y. J. Su and T. H. Ko, *Fuel*, **87**, 2420 (2008).
2. Y. Tang, W. Yuan, M. Pan, Z. Li, G. Chen and Y. Li, *Appl. Energy*, **87**, 1410 (2010).
3. X. Zhang, J. Guo and J. Chen, *Energy*, **35**, 5294 (2010).
4. C. W. B. Bezerra, L. Zhang, H. Liu, K. Lee, A. L. B. Marques, E. P. Marques, H. Wang and J. Zhang, *J. Power Source*, **173**, 891 (2007).
5. W. Trongchuankij, K. Pruksathorn and M. Hunsom, *Appl. Energy*, **88**, 974 (2011).
6. S. S. Kocha, *Electrochemical degradation: Electrocatalyst and support durability*, Polymer electrolyte fuel cell degradation. In: Mench MM, Kumbur EC, Nejat Veziroglu T (Eds.) Massachusetts, Elsevier (2011).
7. N. A. Vante and H. Tributsch, *Nature*, **323**, 431 (1986).
8. J. L. Fernández, V. Raghuveer, A. Manthiram and A. J. Bard, *J. Am. Chem. Soc.*, **127**, 13100 (2005).
9. V. S. Bagotsky, Fuel cells, Problems and Solution. Chichester, UK, Wiley (2009).
10. F. Yongjun and A. V. Nicolas, *Phys. Status Sol.* B, **245**, 1792 (2008).
11. L. Zhang, J. Zhang, D. P. Wilkinson and H. Wang, *J. Power Source*, **156**, 171 (2006).
12. D. Baresel, W. Sarholz, P. Scharner and J. Schmitz Bunsen-Ges, *Phys. Chem. Chem.*, **78**, 608 (1974).
13. D. Susac, A. Sode, L. Zhu, P. C. Wong, M. Teo, D. Bizzotto, K. A. R. Mitchell, P. R. Parsons and S. A. Campbell, *J. Phys. Chem. B.*, **110**, 10760 (2006).
14. K. Lee, L. Zhang and J. Zhang, *Electrochem. Com.*, **9**, 1704 (2007).
15. H. Zhong, H. Zhang, G. Liu, Y. Liang, J. Hu and B. Yi, *Electrochem. Com.*, **8**, 707 (2006).
16. H. Zhong, H. Zhang, Y. Liang, J. Zhang, M. Wang and X. Wang, *J. Power Source*, **164**, 572 (2007).
17. F. Charreteur, F. Jaoeun, S. Ruggeri and J. Dodelet, *Electrochim. Acta*, **53**, 2925 (2008).
18. X. Wang, J. S. Lee, Q. Zhu, L. Liu, Y. Wang and S. Dai, *Chem. Mater.*, **22**, 2178 (2010).
19. J. H. Kim, A. Ishihara, S. Mitsushima, N. Kamiya and K. I. Ota, *Chem. Lett.*, **36**, 514 (2007).
20. C. W. B. Bezerra, L. Zhang, K. Lee, H. Liu, J. Zhang, Z. Shi, A. L. B. Marques, E. P. Marques, S. Wu and J. Zhang, *Electrochim. Acta*, **53**, 7703 (2008).
21. S. L. Gojkovic, S. Gupta and R. F. Savinell, *Electrochim. Acta*, **45**, 889 (1999).
22. O. Contamin, C. Debiemme-Chouvy, M. Savy and G. Scarbeck, *J. New Mater. Electrochem. Syst.*, **3**, 67 (2000).
23. H. Schulenburg, S. Stankov, V. Schunemann, J. Radnik, I. Dorbandt, S. Fiechter, P. Bogdanoff and H. Tributsch, *J. Phys. Chem. B*, **107**, 9034 (2003).
24. C. Medard, M. Lefevre, J. P. Dodelet, F. Jaouen and G. Lindbergh, *Electrochim. Acta*, **51**, 3202 (2006).
25. R. Baker, D. R. Wilkinson and J. Zhang, *Electrochim. Acta*, **53**, 6906 (2008).
26. S. Pylypenko, S. Mukherjee, T. S. Olson and P. Atanassov, *Electrochim. Acta*, **53**, 7875 (2008).
27. U. I. Koslowski, I. Abs-Wurmbach, S. Fiechter and P. Bogdanoff, *J. Phys. Chem. C*, **112**, 15356 (2008).
28. I. Herrmann, U. I. Kramm, S. Fiechter and P. Bogdanoff, *Electrochim. Acta*, **54**, 4275 (2009).
29. V. Jalan and E. J. Taylor, *J. Electrochem. Soc.*, **130**, 2299 (1983).
30. M. T. Paffett, G. J. Berry and S. Gottesfeld, *J. Electrochem. Soc.*, **135**, 1431 (1988).
31. B. C. Beard and P. N. Ross, *J. Electrochem. Soc.*, **137**, 3368 (1990).
32. T. Toda, H. Igarashi, H. Uchida and M. Watanabe, *J. Electrochem. Soc.*, **146**, 3750 (1993).
33. N. R. Elezovic, B. M. Babic, V. R. Radmilovic, L. M. Vracar and N. V. Krstajic, *Electrochim. Acta*, **54**, 2404 (2009).
34. A. Bauer, C. Song, A. Ignaszak, R. Hui, J. Zhang, L. Chevallier, D. Jones and J. Rozière, *Electrochem. Acta*, **55**, 8365 (2010).
35. S. Y. Huang, P. Ganesan and B. N. Popov, *Appl. Catal. B*, **96**, 224 (2010).
36. M. Chisaka, A. Ishihara, K. Ota and H. Muramoto, *Electrochim. Acta*, **113**, 735 (2013).
37. S. Limpattayanate and M. Hunsom, *J. Solid State Electrochem.*, **17**, 1221 (2013).
38. S. Y. Huang, P. Ganesan and B. N. Popov, *Appl. Catal. B.*, **102**, 102 (2011).
39. K. Fugane, T. Mori, D. R. Ou, A. Suzuki, H. Yoshikawa, T. Masuda, K. Uosaki, Y. Yamashita, S. Ueda, K. Kobayashi, N. Okazaki, I. Matolinova and V. Matolin, *Electrochim. Acta*, **56**, 3874 (2011).
40. A. Š. Vuk, R. Ješe, B. Orel and G. Dražic, *Int. J. Photoenergy*, **7**, 163 (2005).
41. S. Thanasilp and M. Hunsom, *Electrochim. Acta*, **56**, 1164 (2011).
42. W. Trongchuankij, K. Poochinda, K. Pruksathorn and M. Hunsom, *Renew. Energy*, **12**, 2839 (2010).
43. S. Yin, S. Mu, H. Lv, N. Cheng, M. Pan and Z. Fu, *Appl. Catal. B.*, **93**, 233 (2010).
44. T. Ungar, J. Gubieza, G. Tichy, C. Pantea and T. W. Zerda, *Compos. A*, **36**, 431 (2005).
45. Y. Ra, J. Lee, I. Kim, S. Bong and H. Kim, *J. Power Sources*, **187**,

363 (2009).
46. Z. B. Wang, G. P. Yin, P. F. Shi and Y. C. Sun, *Electrochem. Solid State Lett.*, **9**, A13 (2006).
47. T. Lopes, E. Antolini and E. R. Gonzalez, *Int. J. Hydrogen Energy*, **33**, 5563 (2008).
48. A. Fujishima, K. Hashimoto and T. Watanabe, TiO_2 Photocatalysis, Fundamentals and Applications, Tokyo Japan, BKC Inc. (1990).
49. A. M. Eppler, I. M. Ballard and J. Nelson, *Physica. E.*, **14**, 197 (2002).
50. K. Pomoni, M. V. Sofianou, T. Georgakopoulos, N. Boukos and C. Trapalis, *J. Alloys Comp.*, **548**, 194 (2013).
51. J. Kim, S. M. Lee, S. Srinivasan and C. E. Chamberlin, *J. Electrochem. Soc.*, **142**, 2670 (1995).
52. E. Antolini, L. Giorgi, A. Pozio and E. Passalacqua, *J. Power Source*, **77**, 136 (1999).
53. E. I. Santiago, R. A. Isidoro, M. A. Dresch, B. R. Matos, M. Linardi and F. C. Fonseca, *Electrochim. Acta*, **54**, 4111 (2009).
54. Z. Liu, B. Guo, J. Huang, L. Hong, M. Han and L. M. Gan, *J. Power Sources*, **157**, 207 (2006).
55. A. J. Bard and L. R. Faulkner, *Electrochemical methods: Fundamentals and applications*, 2nd Ed. New York, Wiley (2000).